

- more, high temperatures at depth promote ductile flow, rather than fracture, to relieve stress [H. Jeffreys, *The Earth, Its Origin, History and Physical Constitution* (Cambridge Univ. Press, Cambridge, ed. 2, 1929); H. Jeffreys, *Proc. R. Soc. Edinburgh* **56**, 158 (1936); M. S. Paterson, *Experimental Rock Deformation: the Brittle Field* (Springer-Verlag, New York, 1978)].
2. A. B. Thompson, *Nature* **358**, 295 (1992); S. Kraft, E. Knittle, Q. Williams, *J. Geophys. Res.* **96**, 17997 (1991).
  3. H. W. Green and P. C. Burnley, *Nature* **341**, 733 (1989).
  4. P. C. Burnley, H. W. Green, D. J. Prior, *J. Geophys. Res.* **96**, 425 (1991); H. W. Green, T. E. Young, D. Walker, C. Scholz, *Nature* **348**, 720 (1990).
  5. S. H. Kirby, W. B. Durham, L. A. Stern, *Science* **252**, 216 (1991).
  6. D. C. Rubie and C. R. Ross, *Eos* **73**, 378 (1992).
  7. C. Meade and R. Jeanloz, *Science* **252**, 68 (1991).
  8. To perform a global study of the detailed rupture process of large earthquakes, teleseismic records of body waves generally have proved the most useful, as well as the most abundant, data set. Recent work with near-field, broad-band body waves to study the source, such as those recorded by TERRAScope in southern California, would not be possible on a global scale because of the lack of dense coverage by broad-band seismometers.
  9. J. E. Vidale and H. Houston, *Nature* **365**, 45 (1993).
  10. We used records from the Southern California Seismic Network, the Northern California Seismic Network, or the Washington Regional Seismic Network, depending on the availability of data. The similarity of the waveform produced by stacking records at each of the three arrays for a particular event justifies using the arrays interchangeably according to which array recorded and archived a given event.
  11. During the period from April 1980 to June 1992, 169 earthquakes occurred between 35° and 90° from California, with seismic moments greater than  $1.6 \times 10^{25}$  dyne-cm and depths greater than 100 km. Events with nodal P-wave radiation coefficients ( $<0.1$ ) were excluded, as were a few events for which the end of rupture could not be reliably inferred or for which the rupture appeared to stop and then restart. The remaining 122 events were used in (9) and in the analysis presented here.
  12. The envelope of a time series is given by the square root of the sum of the squares of the time series and its Hilbert transform [E. R. Kanasewich, *Time Sequence Analysis in Geophysics* (Univ. of Alberta Press, Alberta, Canada, 1981)].
  13. The frequency content of our stacks is controlled by the response of the instruments used in the short-period regional arrays, which is peaked between 0.5 and 4 Hz, and the source spectrum, which is peaked in velocity around the corner frequency (which varies from 0.2 to 2 Hz for these earthquakes). Hence, we obtain envelopes of band-limited seismic radiation. The envelope is similar in shape to the source time function if the shape of the source spectrum does not change during the rupture. Only for band-limited radiation can we get a noise-free and detailed picture of the time-dependent rupture.
  14. In this scheme, each envelope is stretched in time so that rupture begins at normalized time 0 and ends at normalized time 1. Use of this scheme to stretch the envelopes before averaging equalizes the durations of the envelopes, removing the effects of earthquake size and duration and preserving only the shape. Thus, the resulting average envelope shape is not affected by changes in fault parameters that affect the duration in a simple way, such as rupture velocity or stress drop under a constant spectral source model. Furthermore, this scheme has the advantage that the first-order effects of directivity (those due to unilateral rupture), which could affect the duration of the stack (and, hence, the duration of the envelope), do not affect the envelope shape.

- Hence, the use of this scheme ensures that the resulting average envelope shape could not be affected much by systematic differences in directivity, if they are present.
15. The shape of the average envelope for the deepest group of earthquakes is consistent with the common practice in source modeling of parameterizing the time function as the convolution of two boxcars (one representing the duration of rupture over the entire fault and the other the duration of slip at a particular point on the fault).
  16. Vidale and Houston (9) measured durations of 122 deep and intermediate earthquakes from stacks and found a decrease in the duration (when corrected for earthquake moment) of about a factor of 2 from 100 to 600 km depth. If the parameters that describe rupture (which include stress drop, fault geometry, the ratio of rupture velocity to shear velocity, and the intermittency of slip) have no systematic trend with depth, durations should decrease with depth at the same rate that the shear velocity increases with depth, according to a simple scaling model. But shear velocity increases only about 20% between 100 and 600 km in depth. Thus, the observation that durations decrease by a factor of 2 requires that one or more of the rupture parameters change significantly with depth. However, a simple increase in stress drop with depth, which would decrease the duration, would not be sufficient to change the envelope shape from asymmetric to symmetric (Fig. 3A). Furthermore, work by Houston and Williams (19) indicates that average stress drops do not change significantly between 100 and 600 km in depth. Nor would an increase with depth in rupture velocity as a proportion of shear velocity, which could explain the decrease in duration with depth, produce the difference in envelope shapes.
  17. Seismic moments are taken from the Harvard Centroid Moment Tensor catalog [A. M. Dziewonowski and J. H. Woodhouse, *J. Geophys. Res.* **88**, 3247 (1983)].
  18. H. Kanamori and D. L. Anderson, *Bull. Seismol. Soc. Am.* **65**, 1073 (1975).
  19. H. Houston and Q. Williams, *Nature* **352**, 520 (1991).

20. D. L. Turcotte and G. Schubert, *Geodynamics* (Wiley, New York, 1982).
21. T. Irfune and A. E. Ringwood, *High-Pressure Research in Mineral Physics*, M. H. Manghnani and Y. Syono, Eds. (American Geophysical Union, Washington, DC, 1987), pp. 231–242; C. B. Agee, *Annu. Rev. Earth Planet. Sci.* **21**, 19 (1993).
22. The lengths relevant to our seismic observations are on the scale of kilometers rather than meters. Thus, variations in properties over kilometers is probably more pertinent than, for example, absolute grain size.
23. Green and Burnley (3), for example, found that, in experiments on germanate olivine under deviatoric stress, spinel-filled anti-cracks (analogous to Mode I cracks in brittle failure [C. Scholz, *The Mechanics of Earthquakes and Faulting* (Cambridge Univ. Press, Cambridge, 1990), chap. 1] appear to link up into throughgoing Mode II and III structures, on which shear slip occurs. This process occurs through the growth and self-organization of the Mode I anti-cracks at the tip of a growing fault and is believed to occur only once on a given planar structure (H. Green, personal communication). The spinel contents of the anti-cracks are spilled into the growing fault zone, giving it a super-plastic rheology. However, after faulting stops the spinel coarsens to a grain size that is no longer super-plastic, and the fault is, therefore, not able to slip again.
24. The incidence of aftershocks is considerably less common for events deeper than 80 km than for shallower events. Below 450 km there is a moderate increase in the incidence of aftershocks compared to events at depths of 80 to 450 km [C. Frohlich, *J. Geophys. Res.* **92**, 13944 (1987)].
25. We thank J. Savage, W. Thatcher, and Q. Williams for comments on the manuscript and D. Farber and H. Green for helpful suggestions. Supported partially by the National Science Foundation and the W. M. Keck Foundation.

3 January 1994; accepted 2 June 1994

## Orientation Selectivity of Cortical Neurons During Intracellular Blockade of Inhibition

Sacha Nelson,\* Louis Toth, Bhavin Sheth, Mriganka Sur

Neurons in the primary visual cortex of the cat are selectively activated by stimuli with particular orientations. This selectivity can be disrupted by the application of antagonists of the inhibitory neurotransmitter  $\gamma$ -aminobutyric acid (GABA) to a local region of the cortex. In order to determine whether inhibitory inputs are necessary for a single cortical neuron to show orientation selectivity, GABA receptors were blocked intracellularly during whole cell recording. Although the membrane potential, spontaneous activity, subfield antagonism, and directional selectivity of neurons were altered after they were perfused internally with the blocking solution, 18 out of 18 neurons remained selective for stimulus orientation. These results indicate that excitatory inputs are sufficient to generate orientation selectivity.

The ability to respond selectively to contours of a particular orientation is a common feature of visual cortical neurons and is believed to underlie the first stages of the perception of form. Attempts to understand the cellular mechanism of orientation selec-

tivity have led to conflicting interpretations. Intracellular recording studies (1–4) have generally supported the hypothesis that orientation selectivity arises from the pattern of convergence of excitatory afferents from the lateral geniculate nucleus (LGN) (5). Other studies, especially those that employ local application of bicuculline, a blocker of receptors for GABA<sub>A</sub>, have demonstrated the importance of inhibition in maintaining selectivity (6, 7). An

Department of Brain and Cognitive Sciences, Massachusetts Institute of Technology, Cambridge, MA 02139, USA.

\*To whom correspondence should be addressed.

unresolved issue is whether inhibitory synapses directly prevent responses to nonoptimal stimuli or whether their effect is mediated indirectly by neighboring interconnected cortical neurons. This distinction is likely to be of general importance in understanding the function of inhibitory circuits throughout the cerebral cortex.

In order to distinguish between direct and indirect effects of cortical inhibition, we developed a method of blocking inhibitory conductances in single cortical neurons by perfusing them intracellularly with pipette solutions that contained cesium fluoride (CsF), did not contain adenosine triphosphate (ATP) or guanosine triphosphate (GTP) (8), and to which we added the chloride-channel blockers picrotoxin (PTX; 4 cells) (9), or 4,4'-diisothiocyanatostilbene-2,2'-disulfonic acid (DIDS; 14 cells) (10). We assessed the efficacy of the inhibitory blockade in several ways. First, we tested *in vitro* the effects of our solutions on voltage-clamped responses to the GABA<sub>A</sub> agonist muscimol and to electrical stimulation of synaptic inputs (11). Rat visual cortical neurons perfused internally with control solution had large inhibitory responses to applied muscimol (Fig. 1A) or to electrical stimulation (Fig. 1, C and D), whereas cells perfused with CsF-DIDS solution had almost no response to the inhibitory agonist (Fig. 1B) and had purely excitatory responses to electrical stimulation (Fig. 1, E and F) (12).

Next, we confirmed that CsF-DIDS also blocked inhibition *in vivo* by attempting to evoke inhibitory responses in cat neurons, both electrically and visually (13). In control cells, electrical stimuli delivered to the LGN resulted in small excitatory postsynaptic potentials (EPSPs) that were largely obscured by overlapping inhibitory postsynaptic potentials (IPSPs) (Fig. 2A) [see also (1, 3)]. In neurons perfused with CsF-DIDS (Fig. 2B), however, electrical stimuli evoked large EPSPs but no IPSPs. Control recordings from simple cells stimulated with stationary light bars showed inhibition when the stimulus was turned "on" in an "off" subfield or when it was turned "off" in an "on" subfield, as previously reported (3, 14). During recordings from neurons perfused with CsF-DIDS or CsF-PTX solutions, however, blockade of inhibition revealed a small underlying excitation at the onset of a light bar in the "off" subfield and at its offset in the "on" subfield (Fig. 2C). These results are similar to those observed after iontophoretic application of bicuculline (6) and are consistent with the hypothesis that inhibition contributes to the antagonism between "on" and "off" subfields in cortical simple cells (15).

We tested the effects of intracellular blockade of inhibition on the selectivity of

neurons for the orientation of a fixed or moving bar in 18 cells, including 7 simple cells, 6 complex cells, and 5 additional cells that had not been adequately tested with stationary stimuli to be classified as simple or complex. Both simple cells (Fig. 3A) and complex cells (Fig. 3B) maintained a high

degree of orientation selectivity. In six of the cells tested during inhibitory blockade, we presented stimuli at orientations that varied in increments of 30°. Tuning curves constructed from these responses were similar to those obtained extracellularly from other cells (Fig. 4, A and B). In six addi-

**Fig. 1.** Tests of inhibitory blockade in rat visual cortical neurons that were voltage-clamped *in vitro*. Traces are averages of three (A) or five (B), (C), and (E) responses. In (A) and (B), muscimol (100  $\mu$ M) was applied by puff pipette (arrow). (A) Responses during perfusion with control solution. (B) Largest responses that could be evoked in another cell after 10 min of perfusion with CsF-DIDS solution. Duration of muscimol puff was 60 ms in (B), as compared with 10 ms in (A). (C and E) Synaptic currents evoked by electrical stimulation (arrow) of afferents during 800-ms voltage steps from a holding potential of -52 mV. Step voltages ranged from -82 mV (C) or -97 mV (E) to 23 mV by 15-mV increments. (C), Currents evoked in a cell perfused with control solution were primarily outward at potentials above -60 mV. In this cell and in two others, the quaternary lidocaine derivative QX-314 (10 mM) was added to the control solution to improve the voltage clamp. Similar currents were evoked in cells perfused with control solution not containing QX-314. Peak current (measured at time indicated by filled circle) is plotted against membrane potential in (D). (E) Currents evoked in another cell from the same slice as the cell in (C) and perfused with CsF-DIDS are inward at potentials below 0 mV. For clarity, the response at -97 mV is not shown. Peak current (filled circle) and current at 25 ms after peak (open circle) are plotted as filled and open circles in (F). (G and H) Peak muscimol and synaptic currents evoked at 0 mV. Numbers of cells tested are indicated below each bar.

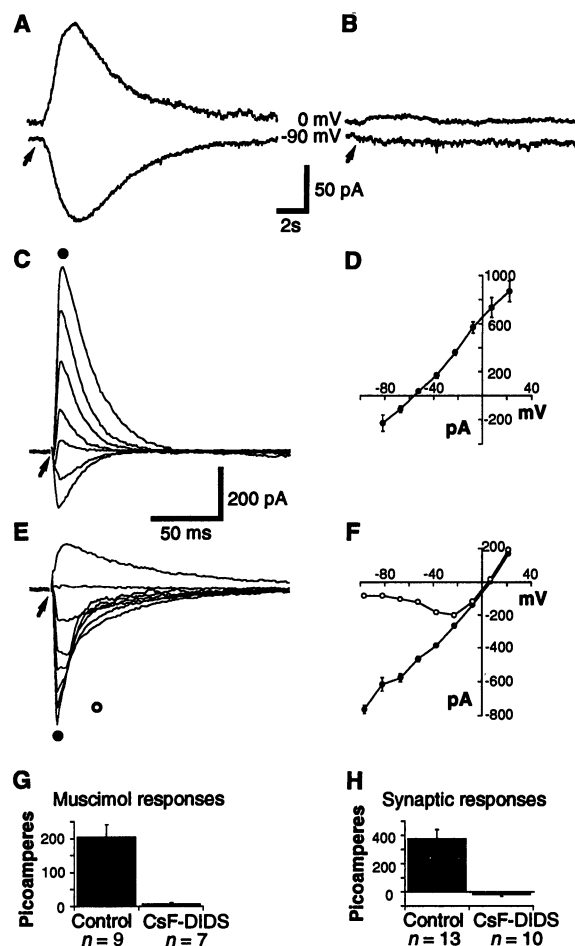
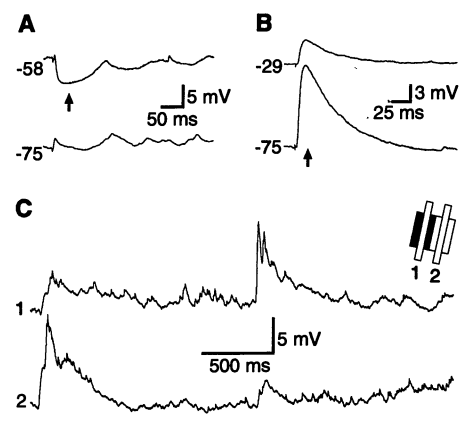


**Fig. 2.** Effects of inhibitory blockade on responses of cat primary visual cortical neurons to electrical and visual stimulation *in vivo*. Each trace is an average of five responses. (A and B) Responses to electrical stimulation (1 mA, 0.1 ms) of the LGN. (A) Control cell response consists of small initial EPSP followed by a large multiphasic IPSP (arrow). (B) Response consists of a large EPSP (arrow), without a subsequent IPSP, in a cell recorded with CsF-DIDS. Electrically evoked IPSPs were observed in all control cells ( $n = 3$ ) and were absent in all cells perfused with CsF-DIDS that were tested ( $n = 6$ ). Four of the cells perfused with CsF-DIDS responded at latencies of 1.6 to 2.0 ms, which indicates monosynaptic input. (C) Responses to visual stimulation with optimally oriented, stationary bars of light presented at two different receptive field locations in a simple cell recorded with CsF-DIDS. Stimulus duration is indicated by the heavy line below trace 2. Membrane potential ( $V_m$ ) = -36 mV.



tional cells, we measured selectivity both extracellularly (while patched on to the cell but before the achievement of whole-cell configuration) and intracellularly (after blockade of inhibition). The degree of orientation selectivity remained similar (Fig. 4, C through E).

The effects of intracellular perfusion on direction selectivity were more heterogeneous. In three of the six cells studied before and after blockade there was an apparent loss of direction selectivity (Fig. 4, F through H). However, some of the remaining 12 cells, which were studied only after blockade, remained quite directionally selective, and overall there was no substantial difference in the distribution of direction selectivities in the blocked and control cells (Fig. 4, F and G). We observed, as

recently reported (15), that spiking responses were often more directionally selective than were subthreshold responses. Hence, loss of directional tuning in some of our cells could have resulted directly from inhibitory blockade (16) or, secondarily, from membrane depolarization.

Although we observed changes in spontaneous firing as well as in electrically and visually evoked synaptic responses that were indicative of the effective blockade of inhibition, we did not observe any substantial change in orientation selectivity. Our results are consistent with the hypothesis that the orientation selectivity of cortical neurons is due primarily to the pattern of convergent excitatory input they receive from thalamic afferents (1, 5) and from other cortical neurons (17). Our results are

not consistent with the hypothesis that inhibitory synapses selectively counteract the effect of excitation at non-optimal orientations. The apparent discrepancy between our data and those obtained when GABA receptors are blocked by application of antagonists to a local region of the visual cortex (6, 7) may reflect the importance of inhibition in regulating recurrent cortical excitation (17). We hypothesize that inhibition evoked at near optimal orientations may help to raise the cell's threshold for firing, thus sharpening the spike response to more broadly tuned excitatory input (18). In our experiments, the firing threshold was presumably maintained near a normal level, despite inhibitory blockade, by the intracellular injection of hyperpolarizing current. Because cortical neurons receive the majority of their excitatory input from neighboring cortical neurons (19), the effect of a reduction in the firing threshold in an ensemble of neurons should be more dramatic than the same effect when confined to a single neuron (20).

## REFERENCES AND NOTES

1. D. Ferster, *J. Neurosci.* **6**, 1284 (1986).
2. R. J. Douglas, K. A. C. Martin, D. Whitteridge, *J. Physiol. (London)* **440**, 659 (1991).
3. D. Ferster and B. Jagadeesh, *J. Neurosci.* **12**, 1262 (1992).
4. For opposing views, see O. D. Creutzfeldt, U. Kuhnt, L. A. Benevento, *Exp. Brain Res.* **21**, 251 (1974); M. Volgushev, X. Pei, T. R. Vidyasagar, O. D. Creutzfeldt, *Visual Neurosci.* **10**, 1151 (1993).
5. D. H. Hubel and T. N. Wiesel, *J. Physiol. (London)* **160**, 106 (1962); B. Chapman, K. R. Zahs, M. P. Stryker, *J. Neurosci.* **11**, 1347 (1991).
6. A. M. Sillito, *J. Physiol. (London)* **250**, 305 (1975).
7. \_\_\_\_\_, *ibid.* **289**, 33 (1979); \_\_\_\_\_, J. A. Kemp, J. A. Milson, N. Berardi, *Brain Res.* **194**, 517 (1980); S. B. Nelson, *J. Neurosci.* **11**, 369 (1991).
8. GABA<sub>A</sub>-mediated chloride conductances are diminished in the absence of intracellular ATP [A. Stelzer, A. R. Kay, R. K. S. Wong, *Science* **241**, 339 (1988); T. Shirasaki, K. Aibara, N. Akaike, *J. Physiol. (London)* **449**, 551 (1992); L. J. Borg-Graham, thesis, Massachusetts Institute of Technology, (1992)] and by intracellular fluoride ions [N. Akaike, N. Inomata, T. Yakushiji, *J. Neurophysiol.* **62**, 1388 (1989)]. GABA<sub>B</sub>-mediated potassium conductances are blocked by intracellular cesium ions [T. S. Otis, Y. De Konink, I. Mody, *J. Physiol. (London)* **463**, 391 (1993)].
9. N. Akaike, K. Hattori, Y. Oomura, D. O. Carpenter, *Experientia* **41**, 70 (1985); R. Metherate and J. H. Ashe, *J. Neurosci.* **13**, 5312 (1993).
10. G. Mathews, E. Neher, R. Penner, *J. Physiol. (London)* **418**, 131 (1989); S. Kokubun, A. Saigusa, T. Tamura, *Pflug. Arch. Eur. J. Physiol.* **418**, 204 (1991); T. Yakushiji, N. Tokutomi, N. Akaike, D. O. Carpenter, *Neuroscience* **22**, 1123 (1987).
11. Techniques for whole cell tight-seal recording in slices were based on published reports [M. G. Blanton, J. J. Lo Turco, A. R. Kriegstein, *J. Neurosci. Methods* **30**, 203 (1989)]. Slices 400  $\mu$ m thick, prepared from the primary visual cortex of rats 3 to 6 weeks old, were maintained at the surface of oxygenated artificial cerebrospinal fluid at 35°C. Control solution contained 120 mM potassium gluconate, 10 mM KCl, 10 mM Hepes, 5 mM EGTA, 3 mM ATP, 2 mM MgSO<sub>4</sub>, and 1 mM GTP. CsF-DIDS solution contained 120 mM CsF, 10 mM KCl, 10 mM Hepes, 5 mM EGTA, and 0.5 to 1 mM DIDS. Solutions were 270 to 280 mosm

**Fig. 3.** Responses of cells in area 17 of the cat visual cortex to moving bars of light during inhibitory blockade of a simple cell (A) and a complex cell (B). Stimuli were moved through the receptive field at the optimal orientation and direction of motion (preferred) or at 90° to the optimal orientation and direction of motion (orthogonal).  $V_m = -39$  mV (A),  $-66$  mV (B). Responses to three stimulus repetitions are overlaid in each panel.

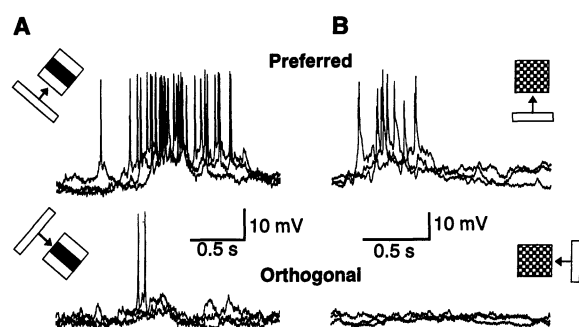
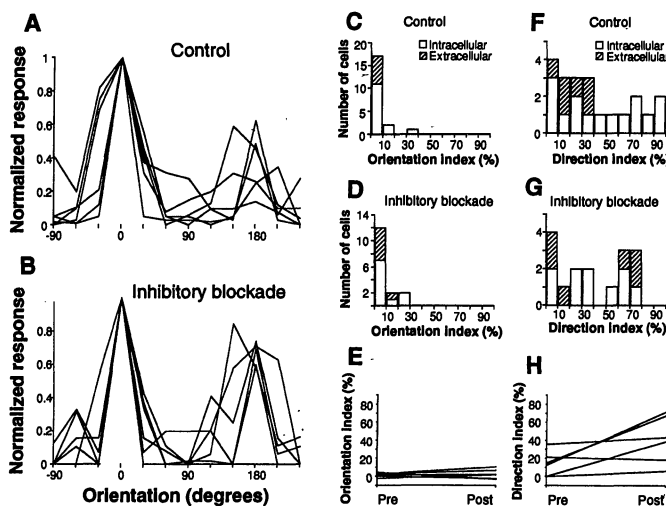


**Fig. 4.** Effects of inhibitory blockade on orientation and direction selectivity. Each stimulus was repeated five times, and responses were averaged, corrected for spontaneous activity, and normalized to the preferred response. Spontaneous firing of control cells was  $0.29 \pm 0.17$  impulses per second. During inhibitory blockade, constant hyperpolarizing current was used to bring spontaneous firing to  $1.16 \pm 0.47$  impulses. (A and B) Orientation tuning curves of six cells recorded extracellularly (A) and of six other cells recorded during intracellular blockade of inhibition (B). Responses are plotted against the stimulus orientation (expressed as degrees from preferred). (C through E) Orientation indices (normalized orthogonal response expressed as percent). (F through H) Direction indices (normalized null response expressed as percent). Control cells (C and F) include cells recorded intracellularly with control solution (open bars;  $n = 14$ ) and cells recorded extracellularly before intracellular blockade of inhibition (hatched bars;  $n = 6$ ). In (D and G), hatched bars represent same cells ( $n = 6$ ) shown in hatched bars of (C) and (F) but after intracellular blockade of inhibition. For these cells, the response at the orthogonal orientation was  $0.2 \pm 1.6\%$  of that elicited at the preferred direction before intracellular perfusion and was  $3.0 \pm 5.4\%$  afterward (mean  $\pm$  SD,  $P = 0.21$ , paired  $t$  test). Remaining cells recorded during inhibitory blockade ( $n = 10$ ) are indicated by open bars. Two cells for which quantitative tests were done only while they were kept sufficiently hyperpolarized to prevent spiking are not included. (E and H) show individual orientation and direction indices for the six cells shown in the hatched bars of (C), (D), (F), and (G), recorded extracellularly (pre) and after intracellular blockade of inhibition (post).



- with a pH of 7.4. Currents were recorded with an Axopatch 200 (Axon Instruments, Foster City, CA) with 70 to 90% compensation of the 10 to 50-megohm series resistance. In each slice, we recorded the responses of at least one control cell. In experiments in which muscimol was applied, each cell perfused with CsF-DIDS was tested with puffs applied at three or more different locations near the recording electrode. Synaptic currents were evoked at a frequency of 0.2 Hz by means of bipolar electrodes placed near the recording site. Stimulus intensity (0.1 to 1.5 mA for 0.1 ms) was adjusted to yield maximal responses.
12. Electrically evoked inhibitory currents contained a large monosynaptic component that persisted in control cells ( $n = 5$ ) during a bath application of 10  $\mu\text{M}$  6-cyano-7-nitroquinoxaline-2,3-dione (CNQx) and 30  $\mu\text{M}$  D,L-2-amino-5-phosphonovaleic acid (APV). The time course and voltage dependence of the early and late components of the synaptic response of cells perfused with CsF-DIDS closely resembled those of the two components of excitatory postsynaptic currents (EPSCs) previously described in hippocampal [S. Hestrin, R. A. Nicoll, D. J. Perkel, P. Sah, *J. Physiol. (London)* **422**, 203 (1990)] and visual cortical neurons [P. Stern, F. A. Edwards, B. Sakmann, *ibid.* **449**, 247 (1992)]. The late component was blocked by 30  $\mu\text{M}$  APV ( $n = 3$ ). No synaptic response remained when both CNQx and APV were present ( $n = 2$ ).
  13. Anesthesia was initiated with ketamine (30 mg per kilogram of body weight) and xylazine (3 mg/kg), given intramuscularly and maintained with isoflurane (1 to 2%, delivered through a tracheal cannula in a 70:30 mixture of  $\text{N}_2\text{O}$  and  $\text{O}_2$ ). Cats were paralyzed with intravenous gallamine triethiodide (3.6 mg/hour) and artificially respired to maintain end-tidal  $\text{CO}_2$  at 3.5%. An animal's electroencephalograph and heart rate were continuously monitored to ensure adequate anesthesia. Bilateral pneumothorax and cisternal drainage were done to improve stability. Techniques for in vivo whole-cell recording and visual and electrical stimulation were similar to those recently described (3) [X. Pei, M. Volgushev, T. R. Vidyasagar, O. D. Creutzfeldt, *Neuroreport* **2**, 485 (1991)]. Electrodes (tip size, 2  $\mu\text{m}$ ; 4 to 10 megohm resistance) containing control solution (15 cells) or CsF-based solution (see 11), with added DIDS (0.5 mM, eight cells; 2 mM, six cells) or PTX (1 mM, four cells), were advanced down the medial bank of the lateral gyrus 0 to 5 mm posterior to the interaural line. Cells were encountered at depths of 300 to 2000  $\mu\text{m}$ . Seal resistances were  $>1$  gigohm. In most cases, we mapped extracellular responses using hand-held or computer-driven stimuli and classified cells as simple or complex. Responses were recorded by means of an Axopatch 200 in voltage clamp mode (4 cells) or by an Axo-clamp in standard bridge mode (29 cells) and were digitized onto videotape (22 kHz) and onto a 486 computer (1 to 2 kHz). In vivo whole-cell recordings were obtained from 33 neurons in 17 female cats (15 cats aged 8 to 14 weeks and 2 adult cats). Initial membrane potentials were  $-40$  to  $-71$  mV, and input resistances were 80 to 320 megohms. Cells recorded with electrodes containing cesium-based solutions quickly developed depolarized membrane potentials ( $-10$  to  $-35$  mV) and broadened action potentials (duration 10 to 50 ms) lacking afterhyperpolarizations, whereas spontaneous firing increased. For cells recorded with inhibitory blocking solutions, responses used for quantitative comparison were collected at least 15 min after recording began and remained stable for up to 2.5 hours. In most cases, we recorded while applying constant hyperpolarizing current that was sufficient to prevent elevated spontaneous firing.
  14. D. Ferster, *J. Neurosci.* **8**, 1172 (1988).
  15. B. Jagadeesh, H. S. Wheat, D. Ferster, *Science* **262**, 1901 (1993).
  16. A. M. Sillito, *J. Physiol. (London)* **271**, 699 (1977).
  17. R. J. Douglas and K. A. C. Martin, *ibid.* **440**, 735 (1991).
  18. A. B. Bonds, *Visual Neurosci.* **2**, 41 (1989).
  19. E. L. White, *Cortical Circuits* (Birkhäuser, Boston, 1989), p. 69.
  20. We have recently found, in detailed simulations of visual cortical circuitry, that disinhibition in single neurons has little effect on their orientation selectivity if constant hyperpolarizing current is applied, but that disinhibition of a group of interconnected excitatory neurons dramatically impairs selectivity without necessarily causing response saturation [D. Somers, S. B. Nelson, M. Sur, *Soc. Neurosci. Abstr.* **19**, 628 (1993)].
  21. We thank D. Ferster and B. Connors for helpful suggestions and P. Schiller for comments on the manuscript. Supported by National Eye Institute grants EY06363 and EY07023.

3 February 1994; accepted 13 June 1994

## NMR Solution Structure of a Peptide Nucleic Acid Complexed with RNA

Stephen C. Brown,\* Stephen A. Thomson, James M. Veal, Donald G. Davis

Peptide nucleic acids (PNA) incorporating nucleic acid bases into an achiral polyamide backbone bind to DNA in a sequence-dependent manner. The structure of a PNA-ribonucleic acid (RNA) complex was determined with nuclear magnetic resonance methods. A hexameric PNA formed a 1:1 complex with a complementary RNA that is an antiparallel, right-handed double helix with Watson-Crick base pairing similar to the "A" form structure of RNA duplexes. The achiral PNA backbone assumed a distinct conformation upon binding that differed from previously proposed models and provides a basis for further structure-based design of antisense agents.

A novel therapeutic strategy is to titrate the concentration of a target enzyme or receptor by altering its expression either at the transcriptional level (antigene) or translational level (antisense) by means of an agent directed against the nucleic acid sequence encoding the target (1). Although this approach has been shown to work in mammalian and plant cells (2) with the use of natural and modified nucleic acids (3), significant obstacles to using such gene-targeted agents to treat human disease remain unsolved (4). PNAs incorporating the nucleic acid bases adenine, cytosine, thymine, and guanine into a polyamide backbone have been described (5) and are of interest as gene-targeting agents. They are made with standard peptide chemistries fully compatible with automated solid-phase synthesis, bind more tightly to their DNA targets than does the cognate DNA strand, and are sensitive to mismatch (6).

We conducted a nuclear magnetic resonance (NMR) investigation to describe the structure of a PNA-RNA complex containing all four common bases. The sequence GAACTC chosen for the PNA (Fig. 1) is capped with G-C base pairs to improve the stability of the complex. The PNA was synthesized with  $>98\%$  enrichment of  $^{13}\text{C}$  and  $^{15}\text{N}$  nuclei on the backbone (7) of the thymine PNA monomer. In this way, isotope-filtering and isotope-

detecting heteronuclear NMR experiments (8) could facilitate  $^1\text{H}$  resonance assignments and provide more information regarding the structure and dynamics of the PNA backbone.

Titration of PNA GAACTC-K# (*bis*-succinyl) and r(GAGUUC) followed by NMR indicated only a 1:1 complex formed at all ratios, with six imino resonances appearing from reduced solvent exchange rates (Fig. 2A). NMR spectra of the uncomplexed PNA indicated that many conformers were present in slow chemical exchange (Fig. 2C) because of *cis-trans* equilibria about the secondary amide bond,  $\chi_1$ , of each PNA residue, whereas in the PNA-RNA complex only one resonance was detected for each proton (Fig. 2B). These data suggest that the PNA backbone adopts a single  $\chi_1$  conformation when bound to the complementary RNA strand.

A complete set of two-dimensional (2D) homonuclear NMR data (9) provided proton resonance assignments of the PNA-RNA complex by standard methodologies (10). The single thymine residue ( $T_5$ ) was easily identified by both double-quantum (2Q) and total correlation spectroscopy (TOCSY) spectra (9). Observation of strong nuclear Overhauser effect (NOE) cross peaks to two adjacent pyrimidine H5, H6 proton pairs identified these as the flanking cytosine bases  $C_4$  and  $C_6$ . NOE cross peaks between cytosine H5 and 4-NH<sub>2</sub> resonances were followed to the guanine imino proton, whereas NOEs among the six imino resonances and aro-

Glaxo Research Institute, Research Triangle Park, NC 27709, USA.

\*To whom correspondence should be addressed.